Carbohydrate Polymers 321 (2023) 121315

Contents lists available at ScienceDirect

Carbohydrate Polymers

journal homepage: www.elsevier.com/locate/carbpol

Tunable biocomposite films fabricated using cellulose nanocrystals and additives for food packaging

Cong Chen [a,b], Wenjing Sun [c], Jinwu Wang [a,b,d,*], Douglas J. Gardner [a,b]

[a] School of Forest Resources, University of Maine, Orono, ME 04469, United States
[b] Advanced Structures and Composites Center, University of Maine, Orono, ME 04469, United States
[c] Institute of Materials (IMX), École Polytechnique Fédérale de Lausanne (EPFL), Lausanne 1015, Switzerland
[d] Forest Products Laboratory, U.S. Forest Service, 1 Gifford Pinchot Drive, Madison, WI 53726, United States

ARTICLE INFO

Keywords:
Cellulose nanocrystals
Additives
Barrier properties
Films
Food packaging

ABSTRACT

Cellulose nanocrystals (CNCs) are considered a prospective packaging material to partially replace petroleum-based plastics attributed to their renewability, sustainability, biodegradability, and desirable attributes including transparency, oxygen, and oil barrier properties. However, neat CNC films are rigid and too brittle to handle or utilize for packaging applications. Hence different additives, including sorbitol, polyvinyl alcohol (PVA), chitin, and κ-carrageenan (CG) were selected to mix with CNCs for packaging film preparation. The influence of additive categories (plasticizer, nonionic polymer, weak cationic and anionic natural polysaccharide), and their concentrations on the performance of CNC suspensions as well as optical, barrier, mechanical, and thermal properties of CNC films were examined. The morphology and physical characterization including density, equilibrium moisture content, contact angle and water durability of the composite films were also determined. Sorbitol and PVA films had the best visible light transparency; mixing with chitin can effectively improve the water durability of CNC films, and CG changed the CNC film from hydrophilic to hydrophobic. Moreover, all CNC films exhibited sufficient oxygen barrier properties, high PVA content films attained the "very high" barrier grade. Thus, durable CNC films can be obtained by adding proper types and amounts of additives, which provides potential scenarios for practical application of CNC films in food packaging.

1. Introduction

Packaging technology plays a crucial role in maintaining the quality, safety, and integrity of food products during storage and transportation (Marsh & Bugusu, 2007). However, the use of conventional petroleum-based plastics for food packaging has led to a growing concern over resource depletion and environmental pollution (Qasim et al., 2021; Thakur et al., 2018). Despite their exceptional properties, low cost, and good processability, the need for sustainable materials in food packaging applications is becoming increasingly critical (Guillard et al., 2018; Tardy et al., 2022). As a result, there is an urgent need to explore and develop sustainable packaging materials that can effectively replace conventional plastics and contribute to more eco-friendly food packaging.

Cellulose nanocrystals (CNCs), as nanoscale biomaterials, hold a crucial position among natural materials and garner tremendous attention from green packaging research communities (Ahankari et al., 2021; Hubbe et al., 2017). CNCs are typically produced from diverse plant-based sources by acid hydrolysis of cellulose fibers with crystalline domains remaining (Trache et al., 2017) and consist of rod-like particles with several hundred nanometers in length and several nanometers in diameter, resulting in high specific surface area and abundant hydroxyl groups on their surface (Mu et al., 2019; Nagarajan et al., 2021; Trache et al., 2017). Accordingly, transparent CNC films can be readily fabricated from CNC suspensions by solvent casting. CNC films exhibit high transparency and oxygen barrier performance at low humidity conditions, fulfilling the basic requirements of food packaging applications (Hubbe et al., 2017). Although CNC films have excellent oxygen barrier properties, their stiffness and brittleness make them unsuitable for food packaging applications (Chen et al., 2022; Csiszár & Nagy, 2017). Furthermore, CNC films disintegrate quickly when exposed to water (Chen et al., 2022), severely limiting their practical use. Therefore, it is crucial to improve the flexibility and handleability of CNC films while maintaining their oxygen barrier properties to expand their potential

* Corresponding author at: Forest Products Laboratory, U.S. Forest Service, 1 Gifford Pinchot Drive, Madison, WI 53726, United States
E-mail address: jinwu.wang@usda.gov (J. Wang).

https://doi.org/10.1016/j.carbpol.2023.121315
Received 2 June 2023; Received in revised form 8 August 2023; Accepted 17 August 2023
Available online 19 August 2023

applications in the food packaging industry.

Easily accessible hydroxyl groups are abundant on the surface of CNCs, which endows CNCs with outstanding compatibility with other materials. To improve the performance of CNC films, a cost-effective and simple strategy is to combine them with plasticizers or biodegradable polymers. Although various types of chemicals have been used in combination with CNCs, no clear, comprehensive comparisons among additives' effect on the properties of CNC films have been reported. Hence, four different categories of typical additives, including sorbitol (Sor, plasticizer), polyvinyl alcohol (PVA, nonionic polymer), chitin (Ch, natural polysaccharide, weak cationic attributable to partial deacetylation), and κ-carrageenan (CG, anionic natural polysaccharide) with incremental doses (5 %, 10 %, 20 %, and 30 %) were mixed with CNC suspensions for composite film preparation and material property determinations. The chemical structures of the additives, their suspensions with CNCs, and films are displayed in Fig. 1. Sorbitol is one of the most common plasticizers that has been demonstrated to enhance the ductility of CNC films (Chen et al., 2022; Csiszár & Nagy, 2017; Fernandez-Santos et al., 2021; Wei et al., 2021). PVA is a water-soluble polyhydroxy polymer with excellent biocompatibility and biodegradability (Xu et al., 2021). PVAs great film-forming and oxygen barrier properties show huge potential for packaging applications (Oun et al., 2022; Panda et al., 2022). Chitin nanofibers are extracted from crustacean shells with 10–20 nm in width and several microns in length. Chitin can be blended with CNCs to form films exhibiting good gas barrier properties, thereby having been proposed for renewable packaging as well (Satam et al., 2019). Carrageenan is a linear sulfated polysaccharide and one of the most promising phycocolloids for food packaging materials attributable to its excellent film-form ability (Aga et al., 2021; Sedayu et al., 2019). Carrageenan is soluble in water, and therefore can be mixed with CNCs for film fabrication with good compatibility (Kassab et al., 2019; Yadav & Chiu, 2019).

CNCs are commonly used to reinforce polymers as fillers (Gupta et al., 2021; Perumal et al., 2018; Voronova et al., 2015), which have met the challenges of dispersing CNCs in polymer matrices uniformly and the compatibility between cellulose and polymers. In this study, we fabricated CNC-based films by incorporation with other materials attributed to their good compatibility, which means that the CNCs serve as a matrix in our composite films. We have hypothesized that a CNC matrix can preserve the characteristics of dense cellulose films, such as light transparency, gas barriers, mechanical, and thermal properties, while a proper additive can tailor the viscosity of mixed suspensions for better film formation and might have synergistic effects on the prepared CNC-based biocomposite films overcoming some disadvantages of pure cellulose films such as brittleness and sensitivity to moisture. The novelty of this work lies in a comprehensive comparison of the effects of different types of additives and their concentrations on the properties of the CNC films, with a focus on identifying the most effective additives on CNC films to meet the diverse requirements of food packaging applications. As mentioned above, to the best of our understanding, no clear and thorough comparisons of the effects among different categories of additives and a wide range of their concentrations on the properties of CNC films have been addressed together. Therefore, this research presents a promising approach to optimize the performance of CNC-based films for various packaging application requirements, as well as provides valuable insights for future research in the field of biobased packaging materials.

2. Materials and methods

2.1. Materials

A cellulose nanocrystal aqueous suspension with 10.3 wt% concentration was produced by US Department of Agriculture Forest Products Laboratory (Madison, WI) and supplied through the Process Development Center of the University of Maine (Orono, Maine, USA). CNCs have been thoroughly characterized in a previous study (Reid et al., 2017): the average length of CNC particles was 134 ± 52 nm with a width of 7 ± 2 nm; the aspect ratio was determined to be 19; the sulfate half-ester ($-OSO_3^-$) content was 335 mmol kg^{-1} as reported. 130 K average Mw polyvinyl alcohol (99 + % hydrolyzed), D-sorbitol (>98 %), and Kappa-carrageenan (CAS: 11114–20-8) were purchased from Sigma-Aldrich (St. Louis, Missouri, USA). There is one sulfate per disaccharide unit in the κ-carrageenan with actual sulfate content around 20 % (Yadav & Chiu, 2019). And the viscosity-average molecular weight of κ-carrageenan is 430 kDa (Derkach et al., 2018). 5 wt% BiNFi-s ultra-fine chitin nanofibers with a 10–20 nm width and several micrometers length were produced by ultra-high pressure water jet technology (Sugino Machine Limited, Japan). Deionized water was used in this experiment.

2.2. Suspensions preparation and characterization

The CNC suspension was diluted to 2 wt% for further processing. PVA (5 wt%) and CG (3 wt%) solutions were prepared by dissolving

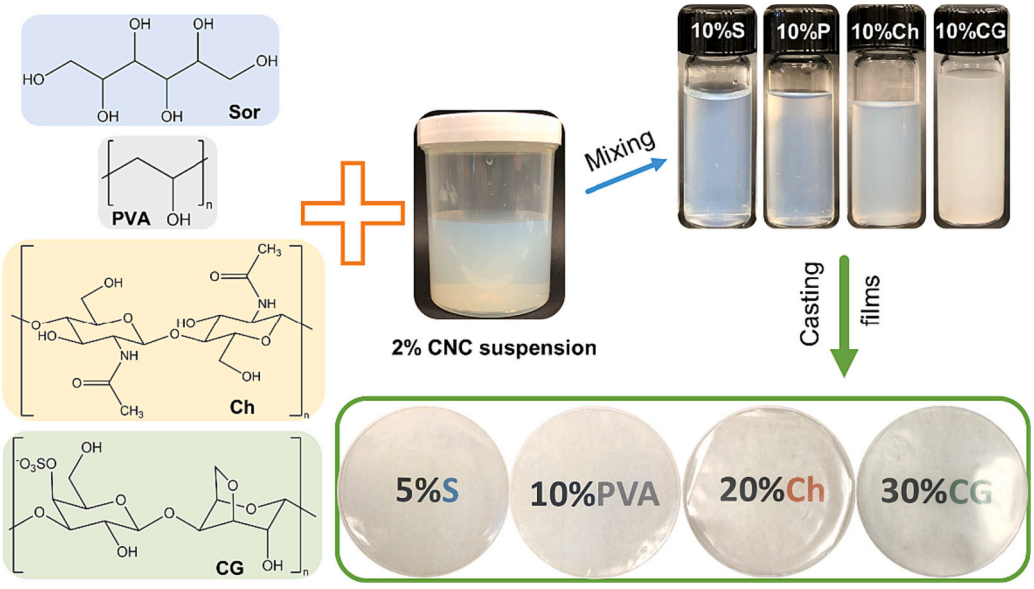

Fig. 1. Schematic representation of CNC-based film preparation, examples of CNC suspensions mixed with 10 % additives, and photographs of CNC composite films.

chemical powders into hot water followed by magnetic stirring and heating. 5 %, 10 %, 20 %, and 30 % CNC-PVA or CNC-CG formulations were obtained by mixing various amount of fresh PVA or CG solution with 2 wt% CNC suspensions, respectively. Sorbitol or chitin nanofibers were directly added into CNC suspensions to obtain CNC-Sor or CNC-Ch formulations, respectively. The suspensions were fully mixed using a T18 digital ULTRA-TURRAX (IKA, Staufen, Germany) at 10 k rpm for 2 min followed by a Thinky 310 planetary mixer (Thinky Corporation, Tokyo, Japan) for 2 min to degas the suspensions. The samples are designated as N%A (where N denotes the concentration number based on CNC dry weight, and A represents the different types of additives). Accordingly, different groups of samples are labeled as 5 % Sor, 10 % Sor, 20 % Sor, 30 % Sor, 5 % PVA, 10 % PVA, 20 % PVA, 30 % PVA, 5 % Ch, 10 % Ch, 20 % Ch, 30 % Ch, 5 % CG, 10 % CG, 20 % CG, and 30 % CG, respectively.

The steady-state viscosity was determined using a Discovery Hybrid Rheometer HR-3 (TA Instruments, New Castle, DE, USA) under a shear ramp mode with a rate increasing from 0.1 to 500 s^{-1} at 23 °C. All formulations were measured using a DIN concentric cylinder geometry.

2.3. Composite film fabrication

Biocomposite films were fabricated using a solvent casting method. The freshly prepared CNC-based suspensions were poured into 100 mm polystyrene petri dishes and dried in a closed fume hood at room conditions. After drying, all films were peeled off from petri dishes and stored in a condition room at 50 % relative humidity (RH) and 23 °C before the material properties testing.

2.4. Optical properties

Visible light transparency of the composite films was measured using a UV − vis spectrometer (Lambda 365, PerkinElmer, Waltham, MA, USA). Air was selected as a reference medium. The optical transmittance value was obtained at 550 nm wavelength.

The optical structural difference of the films was revealed by a polarized optical microscope (POM) (AmScope ME520TA, Irvine, CA, USA). To enhance the birefringence of films, a retardation plate (λ = 530 nm) was added on the microscope.

2.5. Attenuated total reflection Fourier transform infrared (ATR-FTIR)

ATR–FTIR spectra of the film surface were collected on a Spectrum Two FT-IR spectrometer (Perkin Elmer, Waltham, MA, USA). All spectra were obtained using 64 accumulating scans with 4 cm^{-1} resolution over the range from 4000 to 450 cm^{-1}. Spectra were baseline corrected and normalized to the highest peak (set to 1.0).

2.6. Scanning electron microscopy (SEM)

Films were cut and adhered to the SEM stub for surface morphology analysis. Cross sections of CNC films were prepared by the cryofracture method by soaking films in liquid nitrogen. A field-emission scanning electron microscope (FE-SEM) (Zeiss NVision 40, Jena, Germany) was used to represent the morphology of various films. Before imaging, all films, including surfaces and cross-sections, were sputter-coated with a 4-nm gold-palladium conductive layer (Cressington 108 auto Sputter Coater, Cressington Scientific Instruments, UK).

2.7. Equilibrium moisture content

Specimens (1 × 5 cm2) were cut from the films for equilibrium moisture content (EMC) determination. The specimens were placed under 23 °C and 50 % RH conditions; the weight (m_1) was recorded until them reaching the equilibrium state. Then the specimens dried in an oven at 50 °C to obtain the dry weight (m_0), EMC was calculated according to the Eq. (1):

$$EMC\ (\%) = \frac{m_1 - m_0}{m_0} \times 100 \quad (1)$$

Three replicates were tested for each sample, the average value and standard deviation are listed in Table S1.

2.8. Barrier properties

The gas barrier properties of films were evaluated by water and oxygen barrier properties. Water vapor transmission rate (WVTR) and water vapor permeability (WVP) were measured following the ASTM E96/E96M-16 standard. Concisely, films were cut into a 7 cm diameter circular shape and put on the top of Mason jar with around 50 g of deionized water. A silicone rubber gasket and metal screw cap were used to seal the film. The assembled Mason jars were placed in a conditioning room (23 °C and 50 % RH). Weight changes were recorded on 1, 2, 3, 5, and 7 days, WVTR and WVP were calculated using Eqs. (2) and (3), respectively.

$$WVTR\ \left(g\ m^{-2}\ day^{-1}\right) = (G/t)/A \quad (2)$$

where G/t is the slope of the linear section of the mass change-time curve; A is the test area of the film.

$$WVP\ \left(g\ \mu m\ m^{-2}\ day^{-1} kPa^{-1}\right) = \frac{WVTR \times l}{S \times \Delta_{RH}} \quad (3)$$

where S is the saturation vapor pressure at 23 °C (2.81 kPa); l is the thickness of the film; Δ_{RH} is the RH difference inside (100 %) and outside of the jar (50 %).

Oxygen barrier properties were assessed by oxygen transmission rate (OTR) and oxygen permeability (OP). The OTR testing at 50 % RH was carried out using a MOCON oxygen permeation analyzer (OX-TRAN 2/22, Minneapolis, MN, USA) according to the ASTM F1927 standard. OP results were calculated with the following equation:

$$OP\ \left(cm^3\ \mu m\ m^{-2}\ day^{-1} atm^{-1}\right) = OTR \times l/P \quad (4)$$

where P indicates the partial pressure difference of oxygen cross the film.

The average value and standard deviation were based on three replicates of each film sample.

2.9. Water contact angle analysis

The water contact angle (CA) of composite films was measured by a contact angle analyzer (KRÜ SS GmbH, MSA, Hamburg, Germany). 1 μl drop of deionized water was applied on the surface of films. The CA results were collected 2 s after the drop touched the testing surface. Five measurements were carried out for each specimen for the average value and standard deviation.

2.10. Mechanical properties

50 mm × 10 mm specimens were cut from films and placed in the conditioning room (23 °C and 50 % RH) to reach the equilibrium state before measurement. An Instron 5942 universal testing system with a 500-N load cell (Instron, Norwood, MA, USA) was used for examining the mechanical properties, including tensile strength, Young's modulus, strain at break. The crosshead speed was set as 1 mm min^{-1}. The toughness results were obtained by MATLAB (R2022b) according to the strength and strain curve. The average mechanical value and standard deviation of six measurements are reported.

2.11. Thermal stability

A Q500-thermal analyzer (TA Instruments, USA) was used for thermogravimetric analysis (TGA). Around 5 mg samples were tested at a heating rate of 10 °C min^{-1} from room temperature to 600 °C with a 30 ml/min nitrogen flow and 50 ml/ min cooling air flow. The onset degradation temperature and residual content were obtained by TA Universal Analysis.

3. Results and discussion

3.1. Suspension appearance and viscosity

Concentrations of 5 wt%, 10 wt%, 20 wt%, and 30 wt% of sorbitol, PVA, chitin, and carrageenan additives were evenly mixed with the CNC suspensions. The fresh and one-month storage state and dispersion of CNC-additive suspensions are displayed in Fig. S1. All the additives were well dispersed in the fresh CNC suspensions. Adding sorbitol or PVA into CNCs did not significantly influence the visual appearance of the suspensions. The composite suspensions showed semi-transparency and light blue color like the pure CNC suspensions and were not changed by the additive concentration. When mixing with chitin nanofibers, CNC suspensions gradually turned to a milky white color and became opaque as a function of increase in chitin content. The same result was observed for the CNC-CG suspensions but was more obvious compared with CNC-Ch suspensions. The loss of transparency could be attributable to the light scattering from Ch fibers or the large molecular weight CG in the composite suspensions. Additionally, all CNC-Sor and CNC-PVA suspensions still exhibited excellent stability at room conditions after one-month storage. Although fresh CNC-Ch and CNC-CG suspensions displayed good dispersion characteristics, they separated into two phases after standing for one day. The color change and sedimentation of the CNC suspensions after adding Ch and CG indicates the reduction of the repulsive forces among CNCs which commonly occurs when increasing the ionic concentration in a CNC suspension (Arumughan et al., 2021; Cherhal et al., 2015; Guo et al., 2023). These observations agree with the nature of the additives: both Ch and CG are surface charged while sorbitol and PVA are neutral.

Rheological behavior is directly affected by the suspension components. To further characterize the state of prepared suspensions, steady shear viscosity was measured and results are shown in Fig. 2. All Sor and PVA suspensions have low viscosity at around 0.01 Pa·s. There is no notable difference in viscosity across the tested shear rate range with various Sor concentrations (Fig. 2a). The inapparent effect of sorbitol on the viscosity of CNC suspensions is probably attributed to its low molecular weight (Koppolu et al., 2018). The fluctuation at 500 s^{-1} marks the infinite-shear specific viscosity plateau has been reached (Cainglet et al., 2023). Although the viscosities of PVA solutions were reported to clearly increase with polymer concentration (Rošic et al., 2013), the initial viscosity of 5 wt% PVA solution used in this experiment was low, around 0.2 Pa·s. As a result, only a slightly increase in the viscosities of CNC suspensions can be observed when the PVA concentration is raised (Fig. 2b); It was reported that PVA enabled the surfaces of CNCs to slip past each other more easily than those of neat CNCs (Nuruddin et al., 2021) such that at the PVA content levels the viscosity did not change substantially due to the counter effect of the lubricating and polymer entanglement. As for the Ch suspensions (Fig. 2c), the viscosities of 5 % and 10 % Ch were 0.01 and 0.02 Pa·s initially, and did not dramatically decrease within the measured shear rate range. The initial viscosities of CNC suspensions were considerably increased to 0.2 and 2.7 Pa·s at the 20 wt% and 30 wt% Ch concentrations. Moreover, they exhibited steep upturns in viscosity at low shear rates, which indicates a network formation attributed to entanglement between the chitin fibers and CNC particles. As shown in Fig. 2d, the initial viscosities of CG suspensions were about 1 Pa·s, nearly 100 times higher than the Sor and PVA modified CNC suspensions. Viscosity increased evidently by the dosage of CG concentration. All CG samples exhibited the same viscosity change tendency as the function of shear rate in that they displayed a typical shear thinning behavior. The CG suspensions also exhibited upturns towards low shear rates, indicating that there exists a network structure of the suspensions at rest.

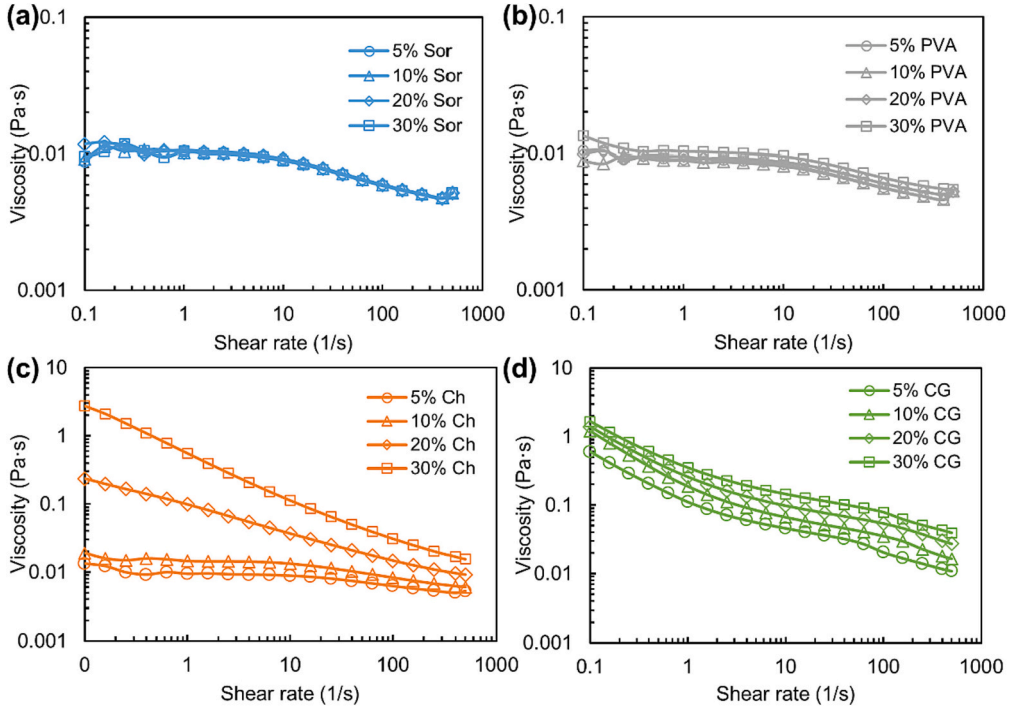

Fig. 2. Steady-state viscosity versus the shear rate of CNC-Sor (a), CNC-PVA (b), CNC-Ch (c), and CNC-CG (d) suspensions at 23 °C.

3.2. Optical properties

UV–vis transmittance of the CNC-additive films was measured within the 200–800 nm wavelength range. All concentrations of Sor and PVA films represented high light transparency with transmittance at 550 nm above 80 % (Fig. 3a, b), except for the 30 % PVA film, which showed lower optical transparency (73 %). In the case of CNC-Ch film (Fig. 3c), transparency decreased from 68 % to 49 % when Ch concentration increased from 5 wt% to 20 wt%. However, transparency increased to 60 % when the Ch concentration further increased to 30 %. The transmittance of CNC-CG mixed films is shown in Fig. 3d. The transparency of 5 %, 10 %, 20 %, and 30 % CG films was 55 %, 60 %, 60 %, and 50 %, respectively. The visual appearance of the CNC composite films with a 10 % concentration is presented in Fig. 3e. The background letters can be seen very clearly throughout all the films. Although some of the mixed suspensions exhibited phase separation during storage as mentioned above, the visible light performance of the resulting films containing CNCs and the various types and concentrations of additives were not significantly affected. This demonstrated excellent optical transparency of composite films, which is an important factor for food packaging applications.

The optical performance of the films was also investigated by polarized optical microscopy (POM) and images are shown in Fig. S2. Cellulose nanocrystals have extrinsic birefringent optical properties (Parker et al., 2018), and can be observed readily by POM (Shrestha et al., 2017). The red, yellow, and blue colors of films result from the 530 nm retardation filter used. Apparent colorful POM images can be obtained from Sor (Fig. S2a) and PVA (Fig. S2b) films, which indicates the typical birefringence from CNCs emergence in the films. However, the birefringence in Ch (Fig. S2c) and CG (Fig. S2d) films is not as obvious as in Sor or PVA films, and the domain size is much smaller in Ch and CG films. According to this visual characteristic, CNC films mixed with Sor or PVA can be considered promising for use in photonic applications.

3.3. ATR-FTIR

To investigate the interaction between the CNCs and the various additives in the films, ATR-FTIR spectroscopy was conducted (Figs. S3,4). The resulting spectra all exhibited the characteristic CNC structure with two distinct regions: one ranging from 2700 to 3500 cm^{-1} and another ranging from 1700 to 600 cm^{-1} (Dassanayake et al., 2021). In particular, the two peaks at 3335 and 3290 cm^{-1} were identified as inter- and intra-molecular hydrogen bonding, respectively. Upon the addition of the different additives, the width and shape of the bands changed. The addition of Sor and Ch resulted in a broader band, while the band became narrower with increased amounts of PVA and CG, indicating that the type and amount of hydrogen bonds changed with

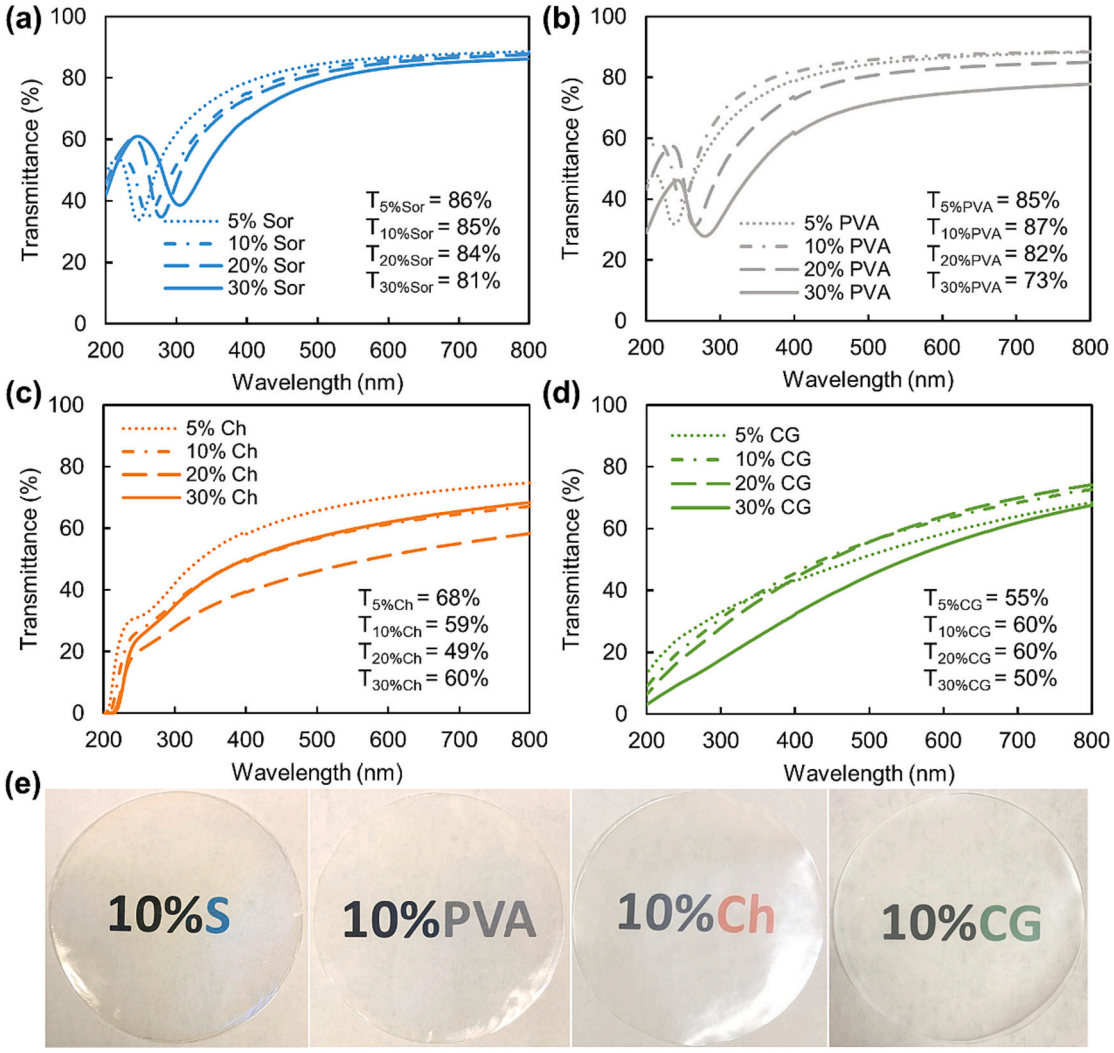

Fig. 3. UV–vis transmittance of CNC-additive: (a) CNC-Sor, (b) CNC-PVA, (c) CNC-Ch, and (d) CNC-CG film, as well as the transmittance values at 550 nm at the right bottom corner of each plot; and (e) optical images of films over their printed designations.

the addition of these additives.

Moreover, the band at around 1640 cm^{-1} was identified as CH_2-O-H bending or H-O-H bending vibration of absorbed water (Dassanayake et al., 2021), with no significant change observed in the Sor, PVA, and CG groups. However, in the Ch group, the band separated into two peaks at 1660 and 1624 cm^{-1} with a new peak at 1560 cm^{-1}, which are typical of Amide *I* and II in chitin structure (Pasquier et al., 2021). The peaks at 867–851 cm^{-1} (galactose-4-sulfate group) are from the CG (Yadav & Chiu, 2019). Another significant observation was that the strong bands in the 1010 to 980 cm^{-1} range decreased in all samples, indicating a change in the structure after incorporating different additives.

3.4. Microstructure of composite films

The effect of additive type and concentration in the CNC films on the morphology and microstructure was examined from FE-SEM surface and cross-sectional images. All films clearly exhibited CNC particles and an ordered nanocrystal arrangement. For the 5 wt% additive concentration, there was no difference in the microstructure of the film surface (Fig. 4a_1- d_1). However, the nanocrystal arrangement dramatically changed as a function of additive concentration, except for Sor, when the concentration increased to 30 wt%. PVA (Fig. 4b_2) and CG (Fig. 4d_2) exhibited a rough surface, and the CG film lost the intrinsic CNC arrangement order. Few chitin fibers were observed on the Ch film surface (Fig. 4c_2), and some holes were apparent on both the Ch and CG films. The defects were probably due to the honeycomb structure forming by the fiber texture and branching of chitin (Satam et al., 2019) or carrageenan.

The CNC arrangement among the different films was further illustrated by the cross-sectional microstructure. The typical highly linear layered CNC film structure was preserved in Sor (Fig. 4a_3) and PVA (Fig. 4b_3) films with small pitch lengths. But this structure disappeared in the Ch (Fig. 4c_3) and CG films (Fig. 4d_3) and the cross sections showed a micro-scaled alignment. This could because Ch and CG have a larger particle size, they dominate in the film structure. However, no big voids were observed, indicating a relatively good interfacial compatibility between the CNC and the additives (Rincón-Iglesias et al., 2020).

The different morphological and microstructural features of the mixture of the CNCs and additives reflect the changing colloidal behavior of aqueous CNC suspensions. Pure CNC suspensions were stable attributable to strong negative surface charges. Anisotropic rod-like CNCs self-assemble into a chiral nematic liquid crystal phase in the suspension and generate a cholesteric CNC film after drying. Small molecular plasticizers diffuse into the cholesteric CNC film, occupy more space, and form hydrogen bonds with the CNCs (Meng et al., 2020). When adding polymers into a CNC suspension, flocculation usually occurs because of polymer adsorption or depletion forces (Oguzlu et al., 2017; Oguzlu & Boluk, 2017). As a neutral polymer with a relatively smaller molecular weight, PVA causes fewer changes on the suspension compared to charged Ch and CG with no visible phase separation and minor morphology change. Contrarily, the oppositely charged Ch led to clear aggregation by electrostatic adsorption and charge neutralization.

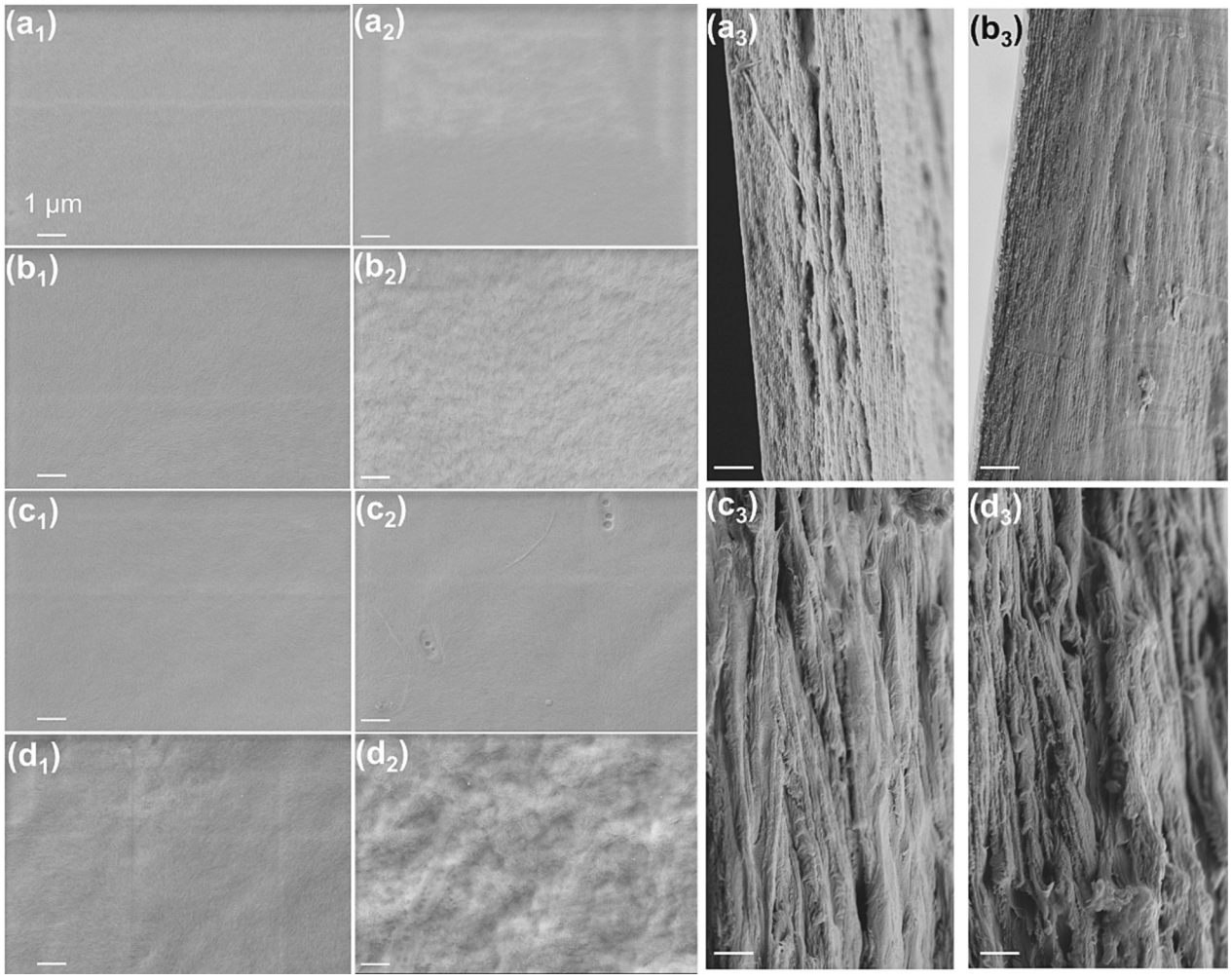

Fig. 4. FE-SEM images of film surface at 10 k magnification: (a_1) 5 % Sor, (b_1) 5 % PVA, (c_1) 5 % Ch, (d_1) 5 % CG, (a_2) 30 % Sor, (b_2) 30 % PVA, (c_2) 30 % Ch, and (d_2) 30 % CG; and cross section of (a_3) 5 % Sor, (b_3) 5 % PVA, (c_3) 5 % Ch, (d_3) 5 % CG films.

Unlike Ch, as an anionic polymer, CG possibly generates sedimentation through depletion flocculation. These changes are also reflected in the properties of the CNC films.

3.5. Physical properties

Physical characteristics of the CNC-based films are listed in Table S1, including thickness, density, and EMC. These properties were all measured for films at 23 °C and 50 % RH. As additive concentration increased in the CNC films, their thickness began to increase. The films containing 5 wt% and 10 wt% additives, as well as the 20 % Sor and CG films maintained a relatively stable thickness of around 30 μm. However, when the Sor or CG content was increased to 30 %, the thickness of these films significantly rose to 36 and 39 μm, respectively. PVA and Ch films showed a relatively high thickness value when the additives content was increased to 20 wt%. The density of the films at 50 % RH varies from 1.4 to 1.5 g cm^{-3}, which is consistent with previous reports (Shrestha et al., 2017; L. Wang et al., 2020). There was no statistical difference among the different samples. The EMC of Sor films gradually decreased from 6.63 % to 5.42 % with an increase in sorbitol concentration. The EMC of PVA, Ch, and CG films showed a decrease with and increase in loading concentration, but increased again after reaching a critical concentration. The inflection point of PVA films is 30 wt%, and of Ch and CG films is 20 wt%. Moreover, the Sor films exhibited a slightly lower EMC corresponding to other films. The EMC decrease could be attributed to the hydrogen bonds forming between CNCs and the additives. The reduction of accessible hydroxyl sites restricts the further hydrogen bonds formed through water molecules at moderate RH (50 %). Although, the average EMC results changed with additives concentrations and types, the statistical difference among different groups, except for 30 % Sor vs 30 % CG, was not significant.

3.6. Barrier properties

Barrier properties are the most critical factor for food packaging materials. The water and oxygen barrier performances of CNC-additive films are shown in Fig. 5. Among the four types of additive-CNC composite films, PVA films showed the best water barrier capability, and a significant reduction of WVTR was observed with increasing PVA content (Fig. 5b). Namely, the 30 % PVA film exhibited the lowest WVTR value, 379 g m^{-2} day^{-1}. This is consistent with a previous study, the 30 % was reported as the optimal PVA loading percentage in CNC coating compositions for water barrier performance because PVA chains fill gaps or form a network with CNCs to minimize the free volume of the films (Chowdhury et al., 2018). The Sor films had better water barrier properties (Fig. 5a), followed by the Ch (Fig. 5c) and CG (Fig. 5d) films. The10% Sor or CG concentration showed a noticeable decrease in WVTR compared with 5 % concentration, however, increasing the amount of Ch did not lead to a significant change in WVTR, possibly because of the exposure to more hydrophilic groups. Although the 5 % Ch film had the poorest water barrier properties, there was no statistical difference among the four loading levels (Table S2). In general, the WVP values of all films were >3000 g μm m^{-2} day^{-1} kPa^{-1} (Fig. S5a), making them classified as poor water barrier films (J. Wang et al., 2018). Because both the CNCs and additives used in this study are natural-based or water soluble, which resulted in relatively unimpressive water barrier properties across all film compositions. According to this point, the composite CNC films probably need to be combined with other post-treatments, such as a lamination with water resistant polymers, for practical food barrier packaging applications. On the other hand, they are promising to use as water vapor permeable films for selective purposes.

CNC films demonstrate a high oxygen barrier performance, which can be attributable to several factors. Firstly, the high crystallinity of CNCs impedes the diffusion of gas molecules. Additionally, strong hydrogen bonds form among the hydroxyl groups on cellulose chains on the surface of CNCs in the film, effectively blocking the movement of gas molecules. Finally, the polarity difference between cellulose and oxygen molecules result in a decrease in oxygen solubility (Chen et al., 2022; L. Wang et al., 2020), further enhancing the oxygen barrier properties of

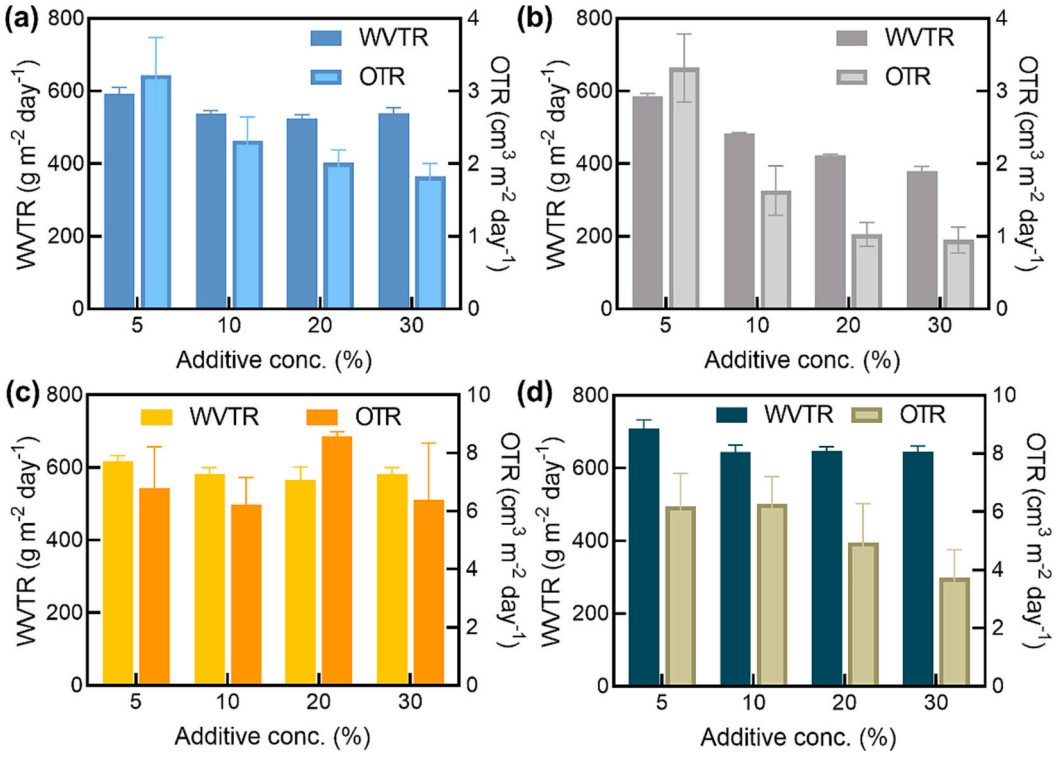

Fig. 5. Water vapor transmission rate (WVTR) and oxygen transmission rate (OTR) results of (a) Sor, (b) PVA, (c) Ch, and (d) CG films measured at 23 °C and 50 % RH.

CNC films. As expected, all the CNC-based composite films demonstrated excellent oxygen barrier properties under 23 °C and 50 % RH conditions (Fig. 5). The Sor and PVA films showed relatively better oxygen barrier properties compared to Ch and CG films. It is speculated that they dispersed very well in CNC suspensions and the available hydroxyl groups could form strong hydrogen bonds with CNC particles to further block the oxygen molecules diffuse through the films. Furthermore, the OP of 20 % and 30 % PVA films were 34 and 37 cm^3 μm m^{-2} day^{-1} atm^{-1} (Fig. S5b), respectively, which falls within the very high oxygen barrier grade (J. Wang et al., 2018). It is believed that the superior oxygen barrier performance of the PVA films can be attributed to the preserved alignment of the CNCs when mixed with PVA, as well as the ability of the PVA to fill the free volume within the interfacial space between CNCs (Nuruddin et al., 2021). Overall, the OP of other films fell within the 40–400 cm^3 μm m^{-2} day^{-1} atm^{-1} oxygen permeability range, which is classified as the high barrier grade. As for the effect of the concentration on the barrier properties, the lowest OTR values were obtained at the 30 wt% loading concentration, with Sor, PVA, and CG films exhibiting OTR values of 1.83, 0.95, and 3.74 cm^3 m^{-2} day^{-1}, respectively; however, the films with 10 wt% Ch addition displayed the best oxygen barrier property among the four concentrations.

3.7. Water resistance

Hydrophilicity is a common characteristic of natural-derived materials, and becomes one of the most challenging issues when used for food packaging applications. Therefore, the CA of different CNC films was investigated (Fig. 6a). Sor, PVA, and Ch showed clear hydrophilicity with a CA value lower than 45°, and no significant difference was observed among the additives loading amounts. This is because they contain numerous hydroxyl groups on their surface, making them inherently hydrophilic. The hydrogen bonds formed by these hydroxyl groups could be easily broken when in contact with water. Moreover, the surface of Sor, PVA, and Ch films are very smooth, which has been displayed in Fig. 4 by SEM images. However, the CG films exhibited surprising CA results. The 5 % CG film had a CA of 78°, when the CG concentration increased to 10 wt%, the CA increased to above 90°. Namely, the 10 %, 20 %, and 30 % CG film surfaces became hydrophobic with CAs all >90°. The excellent hydrophobic performance was probably a result from the rough surface structure since the CA of a pristine CG film is very low (Yadav & Chiu, 2019). The microstructure on the 30 % CG film surface was observed from the SEM micrograph (Fig. 4d_2), and the textured structure of the surface was confirmed as one of the factors that could contribute to the hydrophobic material surface. This is a very interesting result that can be further exploited to increase hydrophobicity of natural biocomposites.

CNC films are highly sensitive to moisture or water and disintegrated immediately after interacting with water (Chen et al., 2022). This shortcoming limits its versatility in food packaging applications. Therefore, the water resistance of the CNC-additive films was investigated after soaking them in water. As shown in Fig. S6 all films maintained their integrity after 1 min of immersion into the water. After 10 mins of soaking, all concentrations of Sor and PVA films completely disintegrated and were barely visible in the petri dish, with PVA films performing slightly better than Sor films. The 5 % to 20 % CG films also started to dissolve into the water and the 30 % CG film kept its initial shape. Chitin films displayed the best water resistance: the 5 % and 10 % films exhibited wrinkling, and the 20 % and 30 % films remained stable. Three hours of soaking led to all films disintegrating except for 20 % and 30 % Ch films, suggesting that adding a proper Ch amount could considerably improve the water durability of CNC films. Thus, mixing CNC with CG or Ch could be a potential way to apply CNC films in moist food packaging applications.

3.8. Mechanical properties

Mechanical properties are essential for food packaging in industrial applications as they prevent premature damage or cracking during transportation, storage, or handling (Yadav & Chiu, 2019). Especially for the CNC films, their rigidity and brittleness, make them difficult to handle. Therefore, the impact of various additives and their content on the mechanical properties of CNC films was examined, and results are displayed in Fig. 7. D-sorbitol has been established as an effective plasticizer that can overcome the brittleness of CNC films (Chen et al., 2022; Csiszár & Nagy, 2017; Fernandez-Santos et al., 2021), and in this study, all Sor films exhibited good flexibility and were easier to handle. The CNC film with 5 wt% content Sor had high tensile strength (71.5 MPa), but its strength decreased sharply as the Sor loading amount increased. The 30 % Sor film had a tensile strength 22.7 MPa, but higher elongation (2.96 %). The large amount of the plasticizer distributed in the CNCs hinders hydrogen bonding among CNCs, which causes CNC particles to slip apart and easily moving under external forces (Csiszár & Nagy, 2017). Meanwhile, the 30 % film showed the lowest stiffness and toughness among all the sorbitol-CNC composite films. All the PVA films exhibited excellent tensile strength (> 75 MPa) and did not decrease significantly with changes in PVA content. It is speculated that the hydroxyl groups on PVA polymer chains interacted well with CNC particles to form strong hydrogen bonds. Furthermore, the strain at break and toughness of PVA films improved with increasing PVA amount. The tensile strength of Ch films did not change significantly under 20 wt%

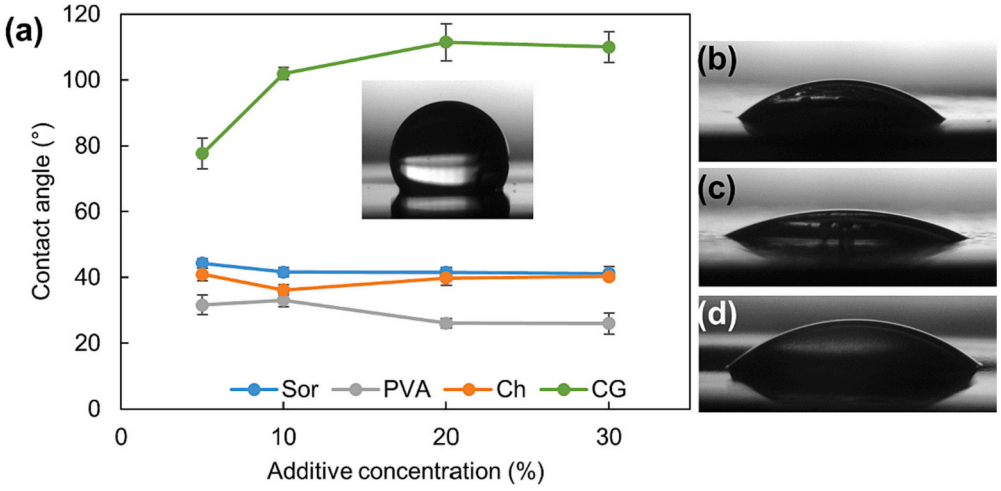

Fig. 6. Contact angle (CA) results (a) of composite films and selected photos of water drop on the 20 % Sor (b), PVA (c), and Ch (d) film surface.

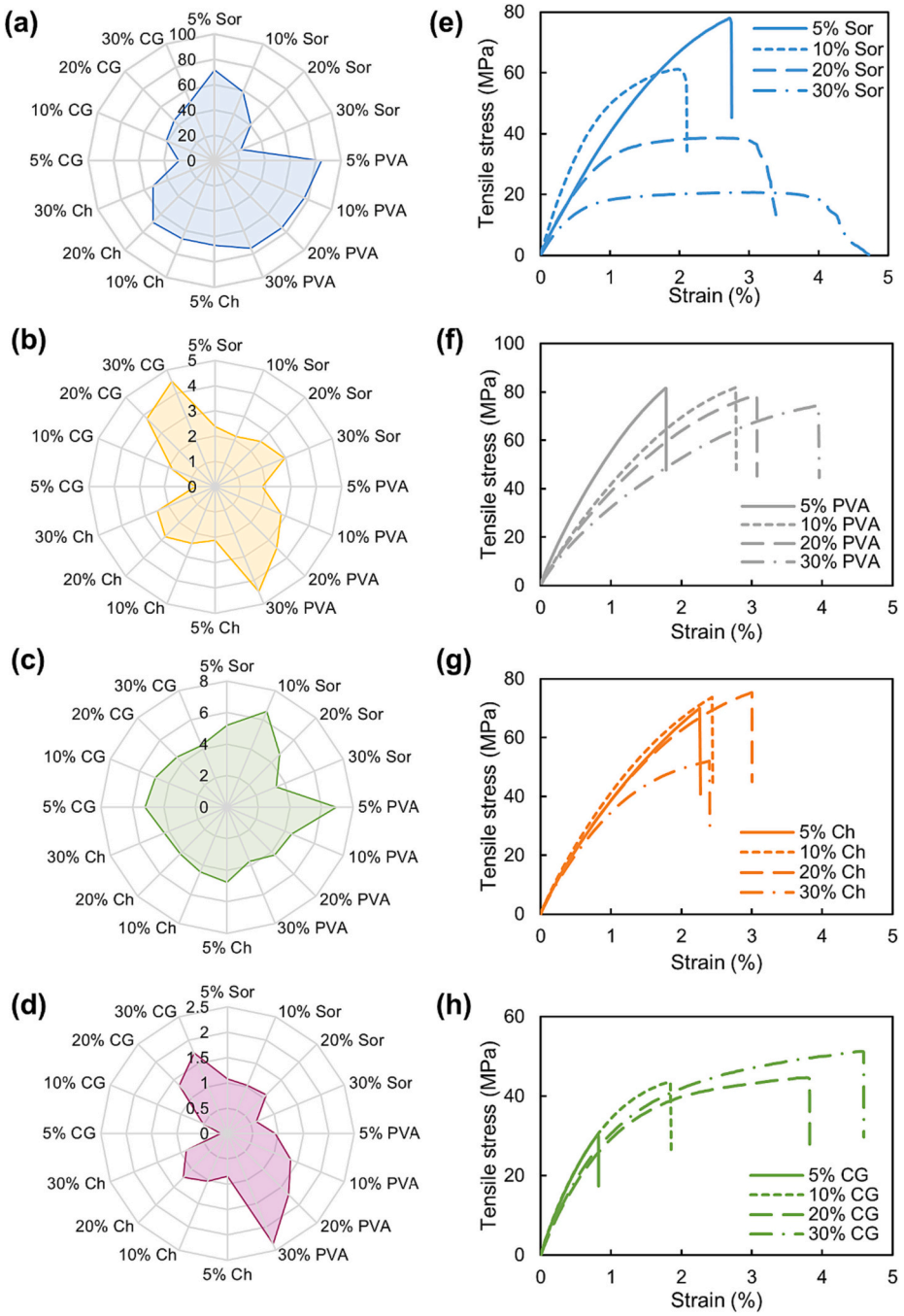

Fig. 7. Mechanical properties results: (a) tensile strength (MPa), (b) tensile modulus (GPa), (c) strain at break (%), and (d) toughness (MJ m^{-3}); representative tensile stress-strain curves of (e) Sor, (f) PVA, (g) Ch, and (h) CG films.

addition. However, it decreased to 52.7 MPa when the chitin concentration was further increased to 30 wt%. The SEM image in Fig. S7 shows several micrometer-long chitin fibers clearly. Therefore, high Ch content in composite films may entangle with CNC particles and inhibit CNCs self-assembling during film drying, leading to a lower tensile strength. The tensile strength, strain at break, and toughness of CG films were continuously increased with increased CG loading, from 28.3 to 50.3 MPa, 0.8 to 4.5 %, and 0.14 to 1.72 MJ m^{-3}, respectively, when CG concentration increased from 5 % to 30 wt%.

3.9. Thermal stability

The thermal stability of the CNC composite films was characterized by TGA (Fig. 8). The derivative thermogravimetric (DTG) results are presented in Fig. S8 and Table S3. Typically, TGA curves of cellulose materials can be divided into three regions: the slight mass loss caused by the water evaporation, the main thermal decomposition result from the cellulose dehydration and depolymerization, followed by the relatively flat region with formation of charred residues (Peng et al., 2013). However, the thermal degradation behavior of CNCs is varied on the resources, preparation conditions, cellulose crystal structures, drying methods, etc. (Dufresne, 2017; Merlini et al., 2020; Peng et al., 2013). In Fig. 8, all samples showed an initial mass loss during the first degradation stage owing to the volatilization of absorbed water, followed by a sharp weight loss. The onset degradation temperature (T_{onset}) of all the films was in the range of 221 to 266 °C (Table S3). As reporting by Reid

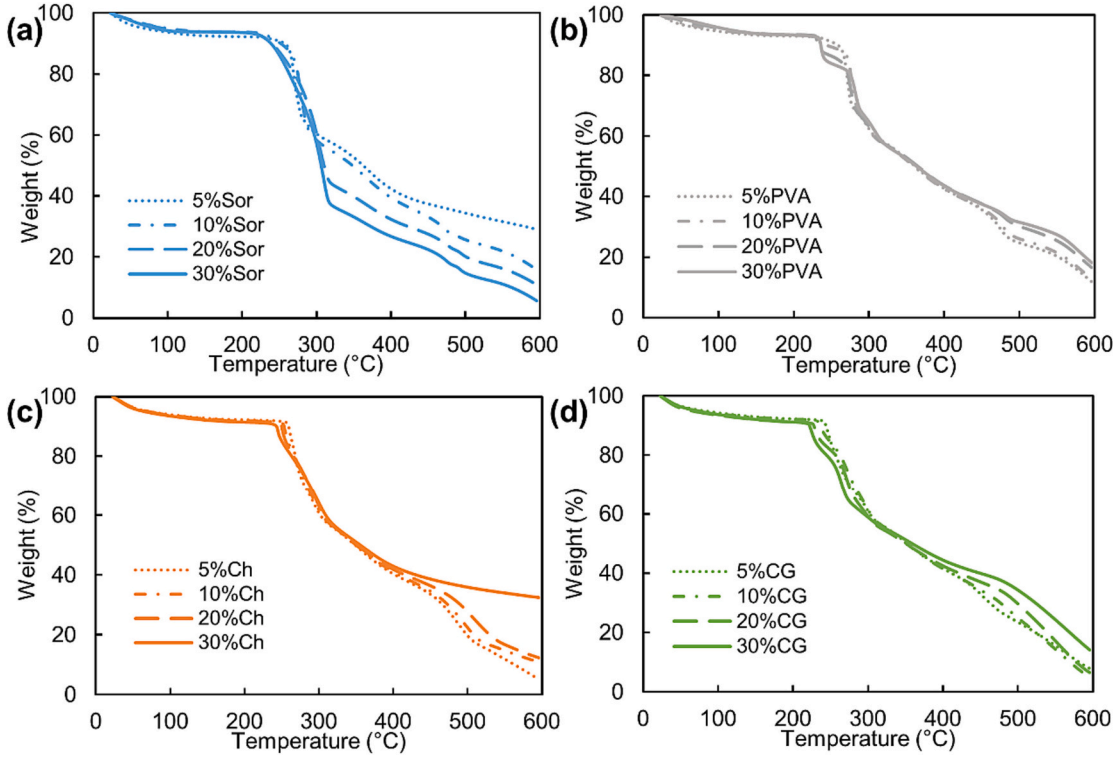

Fig. 8. Thermogravimetric (TGA) curves of CNC films with different amounts (5 %, 10 %, 20 %, 30 %) of (a) Sor, (b) PVA, (c) Ch, and (d) CG additives.

et al. (2017) earlier, the CNCs received from FPL exhibited a typical thermal degradation profile, onset temperature was around 260 °C. Accordingly, different types of additives and their concentrations had a clear influence on the thermal behavior of CNC films. The 5 % and 10 % Sor films showed a relatively high T_{onset} at 263 and 266 °C, but decreased to 233 and 237 °C when sorbitol content increased to 20 wt% and 30 wt%, respectively. For the Ch and CG films, 5 wt% additions resulted in the most thermal stability with the highest degradation temperature (258 and 242 °C) among each group. Generally, the addition of more additives caused CNC films to begin degrading at lower temperatures. Wherein, this effect is more significant in Sor films, and minor in Ch films. However, one more plateau at 235–275 °C in TGA profiles (Fig. 8) was observed for high PVA containing (≥ 10 %) films, corresponding to the peaks (232–237 °C) in DTG curves (Fig. S8 b). This is probably attributable to the onset chain stripping of PVA (Rowe et al., 2016; Sanders et al., 2019). The thermal degradation behavior of CNC films becomes complex when mixed with Ch or CG, which could be reflected in the multiple peaks that emerged in the DTG curves (Fig. S8c, d). Chitin nanofibers showed better thermal stability than CNCs (Irvin et al., 2019), thus, the second degradation peak of Ch films at 300 °C is contributed by the chitin fibers. But CNCs (first peak) were shifted to a lower degradation temperature with higher Ch addition. As for the CG films, carrageenan starts to decompose at lower temperature (150–222 °C) owing to the devolatilization of heavy volatiles (Yadav & Chiu, 2019), which leads to a low onset temperature of composite CNC films. There is an interesting phenomenon, a peak at around 500 °C of 5 % to 20 % Ch films and a broad peak at high temperature appeared in DTG curve, which is uncommon in CNCs, chitin, or κ-carrageenan samples. This thermal degradation behavior of CNC composite films should be further studied in the future. Different from the tendency of onset temperature changes, the residual weights of composite films were increased by the concentration of the increasing additive content except for the Sor samples. The residual weights of PVA and Ch films after TGA testing increased from 11.9 % and 5.2 % to 18.2 % and 32.5 % with 5 % to 30 % addition increase. The 30 % CG also maintained the highest residual weights in the CG group, although the residual weights were nearly similar among the 5, 10, and 20 % CG films. The residual weights of Sor films decreased drastically with an increase in sorbitol content ascribed to the evaporation of the plasticizer (Hansen et al., 2012), which is consistent with previous studies (Ma et al., 2018). In general, the thermal degradation behavior of the CNC films varied from the additive types and concentrations, which indicates the potential for optimizing the thermal properties of CNC based films.

4. Conclusions

In this study, we successfully fabricated high quality CNC based films for food packaging applications by mixing CNCs with four different additives (Sor, PVA, Ch, or CG) at various concentrations (5 wt%, 10 wt %, 20 wt%, or 30 wt%). After characterizing and comparing them based on physical, optical, barrier, mechanical, and thermal properties, we found that the CNC films retained their excellent transparency and intrinsic birefringence when mixed with Sor or PVA. Additionally, CG was able to convert CNC films from hydrophilic to hydrophobic when the concentration reached 10 wt% or higher. Mixing Ch with CNC can improve the water durability of CNC films, making them a promising solution to the water sensitivity issue of CNC films in food packaging applications. Furthermore, the 30 % PVA films exhibited the best barrier properties with 379 g m^{-2} day^{-1} in WVTR and in 0.95 cm^3 m^{-2} day^{-1} OTR at 23 °C and 50 % RH testing conditions, in addition to the good mechanical properties. Accordingly, these eco-friendly CNC based composite films showed the potential for tunable packaging properties by mixing with various types of additives and loading amounts. Through comprehensive study of the characteristics and properties of CNC films affected by different categories of typical additives and their concentrations, valuable insights can be provided for future research when considering CNC films for food packaging applications.

CRediT authorship contribution statement

Cong Chen: Conceptualization, Methodology, Formal analysis, Investigation, Writing – original draft. **Wenjing Sun:** Conceptualization,

Methodology, Validation, Formal analysis, Investigation, Writing – review & editing. **Jinwu Wang:** Conceptualization, Resources, Writing – review & editing, Supervision, Funding acquisition. **Douglas J. Gardner:** Conceptualization, Resources, Writing – review & editing, Supervision, Funding acquisition.

Declaration of competing interest

The authors declare that they have no known competing financial interests or personal relationships that could have appeared to influence the work reported in this paper.

Data availability

Data will be made available on request.

Acknowledgements

This work was supported by the Agriculture and Food Research Initiative Foundational and Applied Science Program grant no. 2018-67010-27906 from the USDA National Institute of Food and Agriculture. The authors gratefully acknowledge Dr. Mehdi Tajvidi and the Laboratory of Renewable Nanomaterials for their generous support in facilitating the laboratory work conducted for this research.

Appendix A. Supplementary data

Supplementary data to this article can be found online at https://doi.org/10.1016/j.carbpol.2023.121315.

References

Aga, M. B., Dar, A. H., Nayik, G. A., Panesar, P. S., Allai, F., Khan, S. A., … Altaf, A. (2021). Recent insights into carrageenan-based bio-nanocomposite polymers in food applications: A review. *International Journal of Biological Macromolecules, 192*, 197–209.

Ahankari, S. S., Subhedar, A. R., Bhadauria, S. S., & Dufresne, A. (2021). Nanocellulose in food packaging: A review. *Carbohydrate Polymers, 255*, Article 117479.

Arumughan, V., Nypelö, T., Hasani, M., & Larsson, A. (2021). Fundamental aspects of the non-covalent modification of cellulose via polymer adsorption. *Advances in Colloid and Interface Science, 298*, Article 102529.

Cainglet, H. E., Tanner, J., Nasiri, N., Browne, C., Garnier, G., & Batchelor, W. (2023). Rapid cellulose nanomaterial characterisation by rheology. *Cellulose, 30*(8), 4971–4982.

Chen, C., Sun, W., Wang, L., Tajvidi, M., Wang, J., & Gardner, D. J. (2022). Transparent multifunctional cellulose nanocrystal films prepared using trivalent metal ion exchange for food packaging. *ACS Sustainable Chemistry & Engineering, 10*(29), 9419–9430.

Cherhal, F., Cousin, F., & Capron, I. (2015). Influence of charge density and ionic strength on the aggregation process of cellulose nanocrystals in aqueous suspension, as revealed by small-angle neutron scattering. *Langmuir, 31*(20), 5596–5602.

Chowdhury, R. A., Clarkson, C., Apalangya, V. A., Islam, S. M. N., & Youngblood, J. P. (2018). Roll-to-roll fabrication of cellulose nanocrystal-poly(vinyl alcohol) composite coatings with controlled anisotropy. *Cellulose, 25*(11), 6547–6560.

Csiszár, E., & Nagy, S. (2017). A comparative study on cellulose nanocrystals extracted from bleached cotton and flax and used for casting films with glycerol and sorbitol plasticisers. *Carbohydrate Polymers, 174*, 740–749.

Dassanayake, R. S., Dissanayake, N., Fierro, J. S., Abidi, N., Quitevis, E. L., Boggavarappu, K., & Thalangamaarachchige, V. D. (2021). Characterization of cellulose nanocrystals by current spectroscopic techniques. *Applied Spectroscopy Reviews*, 1–26.

Derkach, S., Voron'Ko, N., Kuchina, Y. A., Kolotova, D., Gordeeva, A., Faizullin, D., … Makshakova, O. (2018). Molecular structure and properties of κ-carrageenan-gelatin gels. *Carbohydrate Polymers, 197*, 66–74.

Dufresne, A. (2017). *Nanocellulose: From nature to high performance tailored materials*. Walter de Gruyter GmbH & Co KG.

Fernandez-Santos, J., Valls, C., Cusola, O., & Roncero, M. B. (2021). Improving filmogenic and barrier properties of nanocellulose films by addition of biodegradable plasticizers. *ACS Sustainable Chemistry & Engineering, 9*(29), 9647–9660.

Guillard, V., Gaucel, S., Fornaciari, C., Angellier-Coussy, H., Buche, P., & Gontard, N. (2018). The next generation of sustainable food packaging to preserve our environment in a circular economy context. *Frontiers in Nutrition, 5*, 121.

Guo, S., Zhu, Y., Xu, W., Huan, S., Li, J., Song, T., … Rojas, O. J. (2023). Heteroaggregation effects on Pickering stabilization using oppositely charged cellulose nanocrystal and nanochitin. *Carbohydrate Polymers, 299*, Article 120154.

Gupta, V., Yadav, R., Tanwar, R., & Gaikwad, K. K. (2021). κ-carrageenan-based bio-nanocomposite film reinforced with cellulose nanocrystals derived from amla pomace for food packaging. *Biomass Conversion and Biorefinery*, 1–10.

Hansen, N. M., Blomfeldt, T. O., Hedenqvist, M. S., & Plackett, D. V. (2012). Properties of plasticized composite films prepared from nanofibrillated cellulose and birch wood xylan. *Cellulose, 19*(6), 2015–2031.

Hubbe, M. A., Ferrer, A., Tyagi, P., Yin, Y., Salas, C., Pal, L., & Rojas, O. J. (2017). Nanocellulose in thin films, coatings, and plies for packaging applications: A review. *BioResources, 12*(1), 2143–2233.

Irvin, C. W., Satam, C. C., Meredith, J. C., & Shofner, M. L. (2019). Mechanical reinforcement and thermal properties of PVA tricomponent nanocomposites with chitin nanofibers and cellulose nanocrystals. *Composites Part A: Applied Science and Manufacturing, 116*, 147–157.

Kassab, Z., Aziz, F., Hannache, H., Ben Youcef, H., & El Achaby, M. (2019). Improved mechanical properties of k-carrageenan-based nanocomposite films reinforced with cellulose nanocrystals. *International Journal of Biological Macromolecules, 123*, 1248–1256.

Koppolu, R., Abitbol, T., Kumar, V., Jaiswal, A. K., Swerin, A., & Toivakka, M. (2018). Continuous roll-to-roll coating of cellulose nanocrystals onto paperboard. *Cellulose, 25*, 6055–6069.

Ma, X., Qiao, C., Zhang, J., & Xu, J. (2018). Effect of sorbitol content on microstructure and thermal properties of chitosan films. *International Journal of Biological Macromolecules, 119*, 1294–1297.

Marsh, K., & Bugusu, B. (2007). Food packaging—Roles, materials, and environmental issues. *Journal of Food Science, 72*(3), R39–R55.

Meng, Y., Cao, Y., Ji, H., Chen, J., He, Z., Long, Z., & Dong, C. (2020). Fabrication of environmental humidity-responsive iridescent films with cellulose nanocrystal/polyols. *Carbohydrate Polymers, 240*, Article 116281.

Merlini, A., Claumann, C., Zibetti, A. W., Coirolo, A., Rieg, T., & Machado, R. A. (2020). Kinetic study of the thermal decomposition of cellulose nanocrystals with different crystal structures and morphologies. *Industrial & Engineering Chemistry Research, 59*(30), 13428–13439.

Mu, R., Hong, X., Ni, Y., Li, Y., Pang, J., Wang, Q., … Zheng, Y. (2019). Recent trends and applications of cellulose nanocrystals in food industry. *Trends in Food Science & Technology, 93*, 136–144.

Nagarajan, K., Ramanujam, N., Sanjay, M., Siengchin, S., Surya Rajan, B., Sathick Basha, K., … Raghav, G. (2021). A comprehensive review on cellulose nanocrystals and cellulose nanofibers: Pretreatment, preparation, and characterization. *Polymer Composites, 42*(4), 1588–1630.

Nuruddin, M., Chowdhury, R. A., Szeto, R., Howarter, J. A., Erk, K. A., Szczepanski, C. R., & Youngblood, J. P. (2021). Structure–property relationship of cellulose nanocrystal–polyvinyl alcohol thin films for high barrier coating applications. *ACS Applied Materials & Interfaces, 13*(10), 12472–12482.

Oguzlu, H., & Boluk, Y. (2017). Interactions between cellulose nanocrystals and anionic and neutral polymers in aqueous solutions. *Cellulose, 24*(1), 131–146.

Oguzlu, H., Danumah, C., & Boluk, Y. (2017). Colloidal behavior of aqueous cellulose nanocrystal suspensions. *Current Opinion in Colloid & Interface Science, 29*, 46–56.

Oun, A. A., Shin, G. H., Rhim, J.-W., & Kim, J. T. (2022). Recent advances in polyvinyl alcohol-based composite films and their applications in food packaging. *Food Packaging and Shelf Life, 34*, Article 100991.

Panda, P. K., Sadeghi, K., & Seo, J. (2022). Recent advances in poly (vinyl alcohol)/natural polymer based films for food packaging applications: A review. *Food Packaging and Shelf Life, 33*, Article 100904.

Parker, R. M., Guidetti, G., Williams, C. A., Zhao, T., Narkevicius, A., Vignolini, S., & Frka-Petesic, B. (2018). The self-assembly of cellulose nanocrystals: Hierarchical design of visual appearance. *Advanced Materials, 30*(19), 1704477.

Pasquier, E., Beaumont, M., Mattos, B. D., Otoni, C. G., Winter, A., Rosenau, T., … Bras, J. (2021). Upcycling byproducts from insect (fly larvae and mealworm) farming into chitin nanofibers and films. *ACS Sustainable Chemistry & Engineering, 9*(40), 13618–13629.

Peng, Y., Gardner, D. J., Han, Y., Kiziltas, A., Cai, Z., & Tshabalala, M. A. (2013). Influence of drying method on the material properties of nanocellulose I: Thermostability and crystallinity. *Cellulose, 20*, 2379–2392.

Perumal, A. B., Sellamuthu, P. S., Nambiar, R. B., & Sadiku, E. R. (2018). Development of polyvinyl alcohol/chitosan bio-nanocomposite films reinforced with cellulose nanocrystals isolated from rice straw. *Applied Surface Science, 449*, 591–602.

Qasim, U., Osman, A. I., Al-Muhtaseb, A.a. H., Farrell, C., Al-Abri, M., Ali, M., … Rooney, D. W. (2021). Renewable cellulosic nanocomposites for food packaging to avoid fossil fuel plastic pollution: A review. *Environmental Chemistry Letters, 19*(1), 613–641.

Reid, M. S., Villalobos, M., & Cranston, E. D. (2017). Benchmarking cellulose nanocrystals: From the laboratory to industrial production. *Langmuir, 33*(7), 1583–1598.

Rincón-Iglesias, M., Lizundia, E., Costa, C. M., & Lanceros-Méndez, S. (2020). Tailoring electrical and mechanical properties of all-natural polymer composites for environmentally friendlier electronics. *ACS Applied Polymer Materials, 2*(4), 1448–1457.

Rošic, R., Pelipenko, J., Kristl, J., Kocbek, P., Bešter-Rogač, M., & Baumgartner, S. (2013). Physical characteristics of poly (vinyl alcohol) solutions in relation to electrospun nanofiber formation. *European Polymer Journal, 49*(2), 290–298.

Rowe, A. A., M. T., & Gardner, D. J. (2016). Thermal stability of cellulose nanomaterials and their composites with polyvinyl alcohol (PVA). *Journal of Thermal Analysis and Calorimetry, 126*, 1371–1386.

Sanders, J. E., Han, Y., Rushing, T. S., & Gardner, D. J. (2019). Electrospinning of cellulose nanocrystal-filled poly (vinyl alcohol) solutions: Material property assessment. *Nanomaterials, 9*(5), 805.

Satam, C. C., Irvin, C. W., Coffey, C. J., Geran, R. K., Ibarra-Rivera, R., Shofner, M. L., & Meredith, J. C. (2019). Controlling barrier and mechanical properties of cellulose nanocrystals by blending with chitin nanofibers. *Biomacromolecules, 21*(2), 545–555.

Sedayu, B. B., Cran, M. J., & Bigger, S. W. (2019). A review of property enhancement techniques for carrageenan-based films and coatings. *Carbohydrate Polymers, 216*, 287–302.

Shrestha, S., Diaz, J. A., Ghanbari, S., & Youngblood, J. P. (2017). Hygroscopic swelling determination of cellulose nanocrystal (CNC) films by polarized light microscopy digital image correlation. *Biomacromolecules, 18*(5), 1482–1490.

Tardy, B. L., Richardson, J. J., Greca, L. G., Guo, J., Bras, J., & Rojas, O. J. (2022). Advancing bio-based materials for sustainable solutions to food packaging. *Nature Sustainability*, 1–8.

Thakur, S., Chaudhary, J., Sharma, B., Verma, A., Tamulevicius, S., & Thakur, V. K. (2018). Sustainability of bioplastics: Opportunities and challenges. *Current Opinion in Green and Sustainable Chemistry, 13*, 68–75.

Trache, D., Hussin, M. H., Haafiz, M. K., & Thakur, V. K. (2017). Recent progress in cellulose nanocrystals: Sources and production. *Nanoscale, 9*(5), 1763–1786.

Voronova, M. I., Surov, O. V., Guseinov, S. S., Barannikov, V. P., & Zakharov, A. G. (2015). Thermal stability of polyvinyl alcohol/nanocrystalline cellulose composites. *Carbohydrate Polymers, 130*, 440–447.

Wang, J., Gardner, D. J., Stark, N. M., Bousfield, D. W., Tajvidi, M., & Cai, Z. (2018). Moisture and oxygen barrier properties of cellulose nanomaterial-based films. *ACS Sustainable Chemistry & Engineering, 6*(1), 49–70.

Wang, L., Chen, C., Wang, J., Gardner, D. J., & Tajvidi, M. (2020). Cellulose nanofibrils versus cellulose nanocrystals: Comparison of performance in flexible multilayer films for packaging applications. *Food Packaging and Shelf Life, 23*, Article 100464.

Wei, X.-Y., Lin, T., Wang, L., & Yin, X.-F. (2021). Effect of a limited amount of D-sorbitol on pitch and mechanical properties of cellulose nanocrystal films. *Crystals, 11*(11), 1324.

Xu, J.-T., Chen, X.-Q., Shen, W.-H., & Li, Z. (2021). Spherical vs rod-like cellulose nanocrystals from enzymolysis: A comparative study as reinforcing agents on polyvinyl alcohol. *Carbohydrate Polymers, 256*, Article 117493.

Yadav, M., & Chiu, F.-C. (2019). Cellulose nanocrystals reinforced κ-carrageenan based UV resistant transparent bionanocomposite films for sustainable packaging applications. *Carbohydrate Polymers, 211*, 181–194.